atmosphere

Article

Review of the Observed Energy Flow in the Earth System

Chunlei Liu *, Ni Chen, Jingchao Long *, Ning Cao *, Xiaoqing Liao, Yazhu Yang, Niansen Ou, Liang Jin, Rong Zheng, Ke Yang and Qianye Su

South China Sea Institute of Marine Meteorology, Guangdong Ocean University, Zhanjiang 524088, China
* Correspondence: liuclei@gdou.edu.cn (C.L.); longjc@gdou.edu.cn (J.L.); ncao@gdou.edu.cn (N.C.)

Abstract: The energy budget imbalance at the top of the atmosphere (TOA) and the energy flow in the Earth's system plays an essential role in climate change over the global and regional scales. Under the constraint of observations, the radiative fluxes at TOA have been reconstructed prior to CERES (Clouds and the Earth's Radiant Energy System) between 1985 and 2000. The total atmospheric energy divergence has been mass corrected based on ERA5 (the fifth generation ECMWF ReAnalysis) atmospheric reanalysis by a newly developed method considering the enthalpy removing of the atmospheric water vapor, which avoids inconsistencies due to the residual lateral total mass flux divergence in the atmosphere, ensuring the balances of the freshwater fluxes at the surface. The net surface energy flux (F_s) has been estimated using the residual method based on energy conservation, which is the difference between the net TOA radiative flux and the atmospheric energy tendency and divergence. The F_s is then verified directly and indirectly with observations, and results show that the estimated F_s in North Atlantic is superior to those from model simulations. This paper gives a brief review of the progress in the estimation of the observed energy flow in the Earth system, discusses some caveats of the existing method, and provides some suggestions for the improvements of the aforementioned data sets.

Keywords: TOA radiative flux; mass corrected atmospheric energy divergence; net surface energy flux; energy transport

check for updates

Citation: Liu, C.; Chen, N.; Long, J.; Cao, N.; Liao, X.; Yang, Y.; Ou, N.; Jin, L.; Zheng, R.; Yang, K.; et al. Review of the Observed Energy Flow in the Earth System. *Atmosphere* **2022**, *13*, 1738. https://doi.org/10.3390/atmos13101738

Academic Editor: Anthony R. Lupo

Received: 16 September 2022
Accepted: 18 October 2022
Published: 21 October 2022

1. Introduction

The net global radiative flux (F_T) at the top of the atmosphere (TOA) is the difference between the absorbed shortwave radiation and the outgoing longwave radiation of the Earth system, representing the interaction between changes in radiative forcings and climate responses, as well as the influence by unforced variability internal to the climate system [1]. A positive F_T indicates the accumulation of energy in the Earth system and a warming climate.

Satellite observations of CERES (Clouds and the Earth's Radiant Energy System) have provided stable, high-quality TOA radiative energy fluxes since March 2000 [2]. However, this period is short for climate research, so the TOA radiative fluxes since 1985 prior to CERES have been reconstructed [1] by combining earlier satellite observations from ERBE WFOV (Earth Radiation Budget Experiment Satellite wide field of view [3]) and ECMWF (European Centre for Medium Range Weather Forecasts) interim (ERA-Interim) atmospheric reanalysis [4]. Discontinuities in ERBE WFOV observations due to battery failures in 1993 and 1999 were dealt with in the reconstruction using the AMIP5 (5th Atmospheric Model Intercomparison Project) simulations. The reconstruction of TOA radiative fluxes was firstly updated by constraining the fluxes at $10^\circ \times 10^\circ$ resolution using the ERBE WFOV v3.1 data [5], and the latest update used the ERA5 reanalysis [6] and the AMIP6 simulations in 2020 [7].

The net surface energy flux (F_S) has been estimated using the residual method, which is the difference between the net TOA radiative flux and the accumulated total column atmospheric energy divergence and tendency. This method has been widely employed by the community [8] and is believed to be the most accurate way of estimating the F_S since it can ensure the conservation of the energy in the entire atmospheric column [5,7,9–14].

The column-integrated atmospheric energy accumulation and divergence must be obtained as accurately as possible. The atmospheric state close to the real world is from the atmospheric reanalysis due to the assimilation of a large number of observations to the atmospheric numerical forecast model. However, because of the simultaneous assimilation of the three-dimensional wind field and the surface pressure, there is no guarantee for the mass balance in the atmospheric column [9–11]. Therefore, mass correction is needed in order to get the right energy divergence that is closely associated with mass transport. Progress has been made in the mass correction of the atmospheric reanalysis data, particularly after removing the enthalpy of the atmospheric water vapor [12,13], which avoids inconsistencies due to the residual lateral total mass flux divergence in the atmosphere, ensuring the balance of the freshwater fluxes at the surface [7].

By combining the net TOA fluxes with the atmospheric energy accumulation and the mass-corrected horizontal atmospheric energy transport from atmospheric reanalyses, the net surface energy fluxes can be estimated by the residual method [5,10,11,15]. The reconstructed TOA fluxes by Allan et al. [1] and Liu et al. [5,7,11] are regarded as "high confidence" in the IPCC (Intergovernmental Panel on Climate Change) AR6 report (sixth assessment report) [16] (see page 17 of Chapter 7 of the report), and both the TOA fluxes and estimated net surface energy fluxes have been widely used in climate research and model validation by the research community. This data set is normally referenced as DEEPC (or DEEP-C: Diagnosing Earth's Energy Pathways in the Climate system) and can be available at https://researchdata.reading.ac.uk/347/ (accessed on 26 October 2021).

This paper will briefly review the development of the DEEPC data set and the inferred energy flow. Comparisons with RAPID (Rapid Climate Change-Meridional Overturning Circulation and Heat flux array, [17]) observations will be described, and the future work needed for the improvement of this data set will be discussed.

2. Data and Methods

Data sets used in this paper include satellite observations (CERES Ed4.1 and ERBS WFOV v3.0) at TOA, the ERA5 atmospheric reanalysis, ORAS5 (Ocean ReAnalysis System 5, [18]) ocean reanalysis, RAPID observations, the reconstructed DEEPC TOA radiative fluxes, and the estimated net surface energy flux [19], together with ten AMIP6 model simulations. All data set names and brief descriptions are listed in Table 1.

The net surface downward energy flux F_s was originally calculated using the following equation [10,11,20]:

$$F_S = F_T - \frac{\partial E}{\partial t} - \nabla \cdot \frac{1}{g} \int_0^1 \boldsymbol{V}(h+k) \, \frac{\partial p}{\partial \eta} d\eta \tag{1}$$

where F_T is the TOA net radiation flux, E is the total column atmospheric energy and $\partial E/\partial t$ is its tendency. g is the gravitational acceleration, $\boldsymbol{V}$ is the horizontal wind velocity vector, h is the moist static energy, k is the kinetic energy, and p is the pressure. η is the hybrid vertical coordinate and is a function of the atmospheric and surface pressure [21].

Equation (1) has been modified by Mayer et al. [12,13], and the enthalpy of atmospheric water vapor has been removed to ensure the consistency of the atmospheric lateral total mass flux divergence and ensure the balances of the surface freshwater fluxes [7,13]. The updated equation is

$$F_S = F_T - \frac{\partial E}{\partial t} - \nabla \cdot \frac{1}{g} \int_0^{p_s} \left[(1-q_g) C_a (T - T_o) + L_v(T) q_g + \varphi + k \right] \boldsymbol{V} dp \tag{2}$$

where L_v is the latent heat of condensation of water, q_g is the specific humidity, C_a is the specific heat capacity of air at constant pressure, T is the air temperature (relative to reference temperature T_o), and φ is the geopotential energy, respectively.

According to Loeb et al. [7,19,22,23], the column-integrated ocean heat divergence ($\nabla \cdot E_O$) can be calculated from the following equation.

$$\nabla \cdot E_O = F_O - OHCT \tag{3}$$

where F_O is the energy entering the ocean, and the difference between F_S and F_{ice} ($F_O = F_S - F_{ice}$). F_{ice} is the energy from sea ice formation and melting, estimated from five ensemble members of ECMWF's ORAS5 ocean reanalysis [18]. The ocean heat content tendency (OHCT) is calculated from the ocean heat content (OHC) using central differences (e.g., the OHCT in July is the difference of OHCs between August and June and divided by the time difference). Liu et al. [7] calculated the OHCT using the OHC integrated over 0–2000 m. The result shows good agreement in both variability and absolute value with the global mean F_S and is therefore used in this study. The flowchart of data retrieval is displayed in Figure 1.

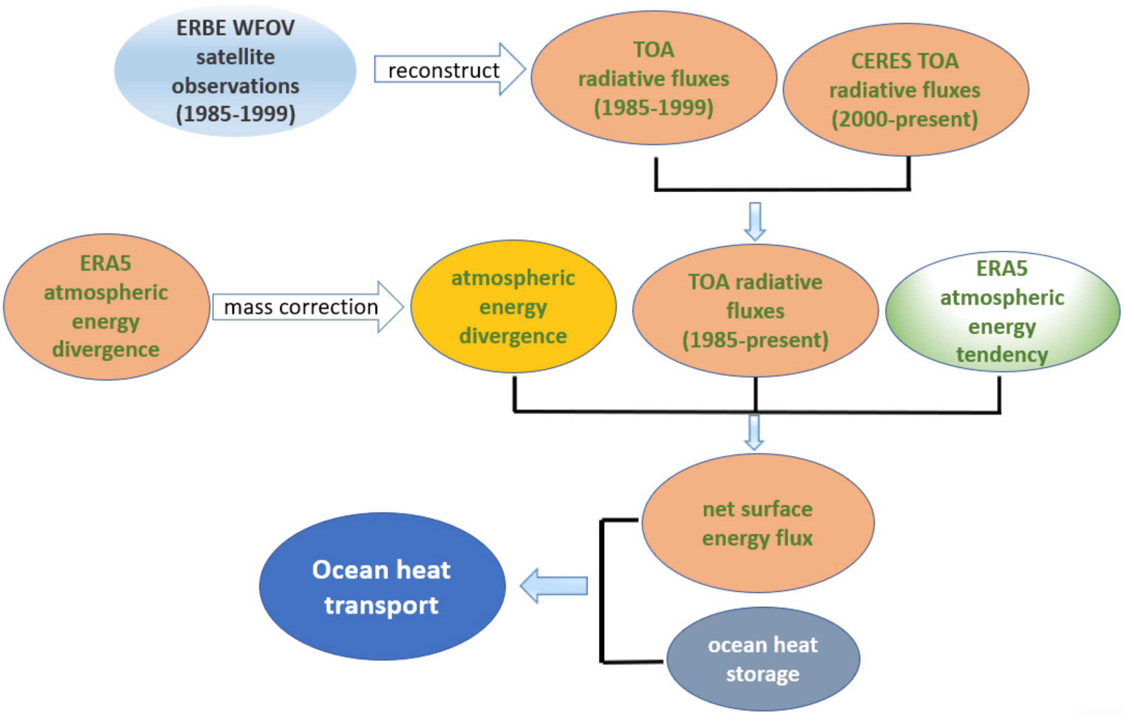

Figure 1. Flowchart of data retrieval.

Table 1. Data sets and brief descriptions.

Data Set	Period (in This Study)	Horizontal Resolution	References
DEEPC v5.0	1985–2017	0.7° × 0.7°	Liu et al. (2020) [7]
WFOV v3.0	1985–1999	10° × 10°	Wong et al. (2006) [3]
CERES Ed4.1	2001–2019	1.0° × 1.0°	Loeb et al. (2018) [24]
RAPID	2004–2017		Smeed et al. (2017) [17]
ERA5	1985–2018	0.25° × 0.25°	Hersbach et al. 2020 [6]
ORAS5	1993–2016	1.0° × 1.0°	Zuo et al. (2019) [18]
AMIP6 simulations:			
BCC-CSM2-MR	1985–2014	1.125° × 1.125°	Wu et al. (2021) [25]
CESM2		0.94° × 1.25°	Danabasoglu et al. (2020) [26]
CNRM-CM6-1		1.40° × 1.40°	Eyring et al. (2016) [27]
EC-Earth3-Veg		0.70° × 0.70°	Davini et al. (2017) [28]
FGOALS-f3-L		1.0° × 1.25°	He et al. (2020) [29]
HadGEM3-GC31-LL		1.25° × 1.875°	Williams et al. (2015) [30]
IPSL-CM6A-LR		1.25° × 1.25°	Boucher et al. (2019) [31]
MIROC6		1.43° × 1.43°	Tatebe et al. (2019) [32]
MRI-ESM2-0		1.125° × 1.125°	Yukimoto et al. (2019) [33]
SAM0-UNICON		0.94° × 1.25°	Park et al. (2019) [34]

3. Results

3.1. Net TOA Radiative Flux

The radiative fluxes at TOA over 1985–1999 are reconstructed using CERES climatology and ERA5 anomalies constrained by the observed ERBE WFOV anomalies in a $10^{\circ} \times 10^{\circ}$ box. The discontinuities in 1993 and 1999 are adjusted based on the AMIP6 ensemble mean differences at both sides of discontinuity points [2,7,11]. The anomaly time series of the monthly global mean net TOA fluxes (NET) is calculated with the reference period from 2001–2005, and the results are plotted in Figure 2. The time series include data from AMIP6 ensemble mean and spread (±one standard deviation), CERES Ed4.1, ERA5, DEEPC, and ERBE WFOV v3.0. The ERBE WFOV data are 72 day means relative to the reference period 1985–1999, and other lines are three-month running means. The ERBE WFOV anomaly line is shifted 0.23 Wm^{-2} downward for clarity. While the multiannual mean NET fluxes over 1985–1999 are 0.10 ± 0.61 Wm^{-2}, it is 0.62 ± 0.10 Wm^{-2} over 2000–2016. The comparison with the results of Cheng et al. [35] shows qualitative consistency. Both the reconstructed and CERES data are regarded as "high confidence" by the IPCC AR6 report. It is noticed that the uncertainty range of 0.61 Wm^{-2} over 1985–1999 is still large, mainly from the spread of the AMIP6 simulations at the discontinuity points around 1999. This large uncertainty needs to be improved in future study.

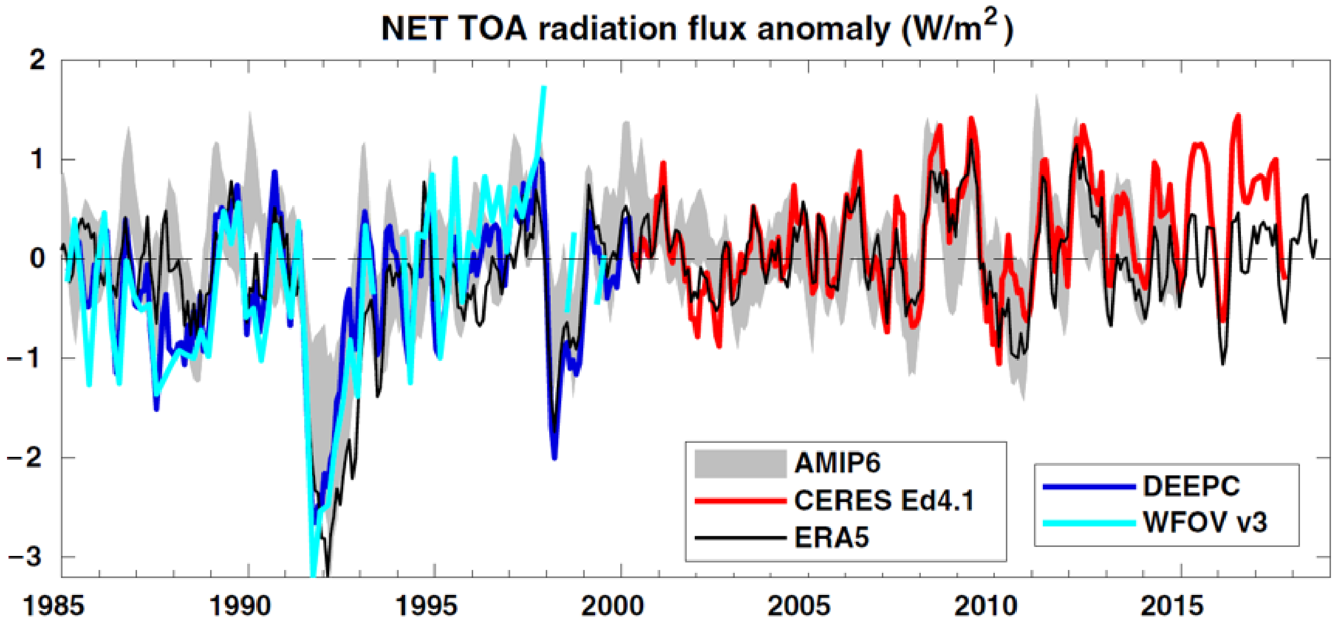

Figure 2. Anomaly time series of the monthly global mean net TOA radiation fluxes (NET) in Wm^{-2}. The reference period for anomaly calculation is 2001–2005. All lines are three-month running means. The WFOV data are 72 day means, and their anomalies are calculated with the reference period of 1985–1999. The WFOV line is shifted 0.23 Wm^{-2} downward for clarity. Gray shading denotes the ±one standard deviation from ten AMIP6 simulations.

It is noticed that the ensemble mean of ten AMIP6 net TOA fluxes has good variability agreement with observations. The ERA5 data have very close co-variations with CERES data before 2012, but the CERES data are larger than the ERA5 after 2012; the reason for this discrepancy is not clear and needs further investigation.

3.2. Energy Flow in the Earth System

Figure 3 is the schematic diagram showing the energy flow in the Earth system. Terms used in the estimation of the net surface energy fluxes are all displayed. The energy flow over land is in the left column, and that over the ocean is in the right column. There is a net energy transport from the ocean to land. The net surface energy flux F_s can be calculated by

Equation (2). The mass-corrected atmospheric energy divergence is from Mayer et al. [13] using ERA5 atmospheric reanalysis. It has been noticed that the estimated global mean F_s over land is unrealistic, so the global land mean F_s over 2004–2014 is anchored to a new estimate of 0.2 Wm^{-2} [36], and the excess/deficit energy fluxes over land are then redistributed over oceans (see [5] for details).

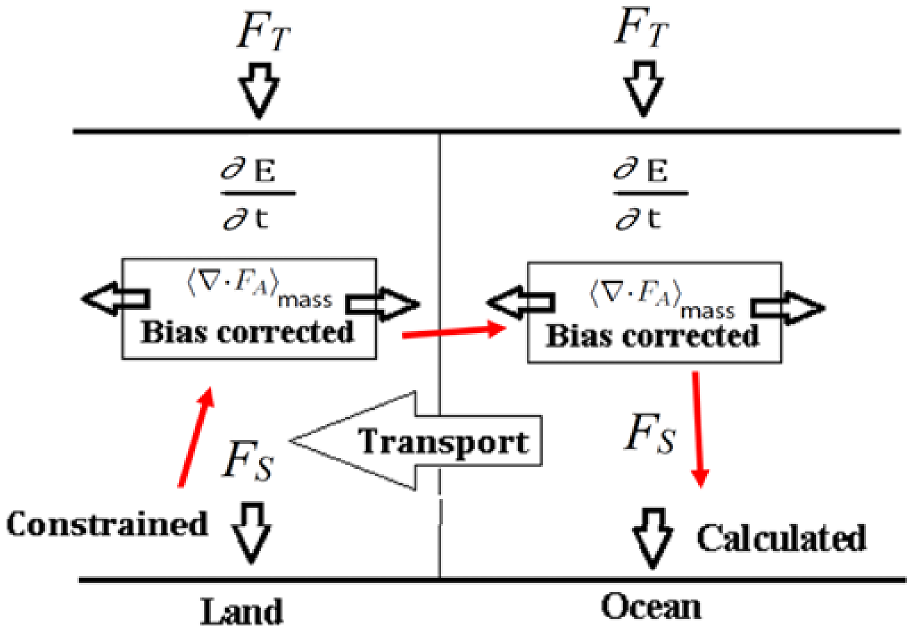

Figure 3. Schematic diagram showing the energy flow in the climate system. The land surface flux is constrained by new observations, the atmospheric divergences over land and ocean are adjusted to respond to this constraint, and the surface energy fluxes can be estimated using the residual method. Red arrows indicate the adjustment sequence after the land surface flux is constrained.

The DEEPC data set includes the TOA radiative fluxes and the net surface energy fluxes, so it can be used to estimate the energy flow in the atmosphere. By combining with the ocean heat content tendency from ORAS5, the ocean heat transport can also be inferred. The energy flow in the Earth system (including the atmosphere and ocean) can be estimated [7,19,22,23].

The latest estimation [7] of the multiannual mean (2006–2013) from DEEPC data shows that there is a gain of 0.36 $\pm$ 0.04 PW net downward radiation flux at TOA in the southern hemisphere, and the net radiation flux at TOA of the northern hemisphere is close to balance. At the surface, there is more net downward energy flux (0.79 $\pm$ 0.16 PW) entering the ocean in the southern hemisphere and net upward energy flux (0.44 $\pm$ 0.16 PW) in the northern hemisphere. Therefore, there is an atmospheric energy divergence in the southern hemisphere and convergence in the northern hemisphere, leading to a net energy flow of about 0.44 $\pm$ 0.16 PW from the northern hemisphere to the southern hemisphere. Considering the ocean heating in the two hemispheres, it can be estimated that the northward heat transport at the equator is about 0.50 $\pm$ 0.16 PW, and it is mainly transported by the Atlantic meridional circulation. Please note that these absolute values of the energy transports can be sensitive to the time period selected.

The oceanic heat transport at 26° N in the Atlantic can be inferred as an indirect check of F_S. The inferred transport can be compared with the RAPID observations. The time series of the transport from RAPID and that inferred from DEEPC surface fluxes, and ocean heat content tendency is plotted in Figure 4. There is a good agreement between the inferred heat transport from DEEPC and the RAPID observation in both quantity and variability. The RAPID observations show 1.22 PW mean heat transports, and the inferred transport from DEEPC is 1.23 PW, respectively. The correlation coefficient between these two time-series is 0.32 over the period from April 2004 to February 2017, and it is 0.73 from

2008–2016. The earlier large discrepancy before 2008 between RAPID data and inferred transport is due to the greater uncertainty in observations [8].

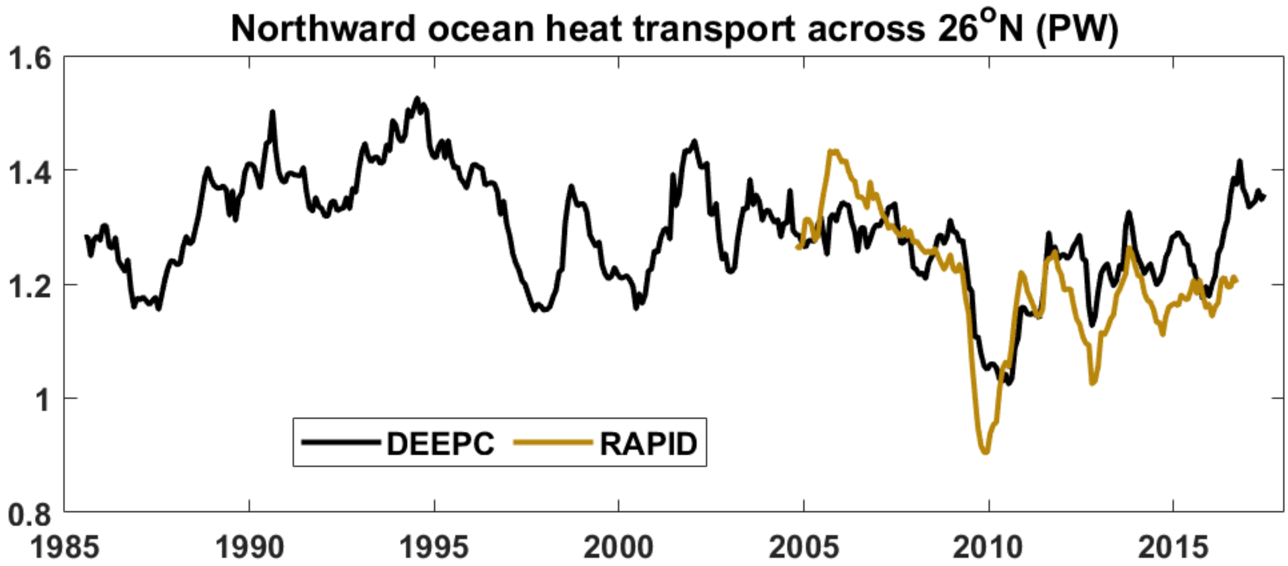

Figure 4. Northward meridional ocean heat transports at 26° N in the Atlantic. The DEEPC net surface fluxes are in black and RAPID observations are in brown.

The net surface flux F_S from the DEEPC data set over the north Atlantic has been compared with those from AMIP6 model simulations [19]. Results show that the inferred northward meridional ocean heat transports derived from AMIP6 F_S over the north Atlantic are all smaller than observations and that from the DEEPC data set, the discrepancy is mainly from the overestimation of the latent heat (evaporation) in AMIP6 simulations. Because the simulations have greater surface wind speed [37], which will enhance the difference between the wind at 10 m and the ocean surface current, increasing the turbulent heat fluxes according to the bulk formula. More detailed investigations are needed over the north Atlantic. It is also found that the model resolution will affect the net surface heat flux. Liu et al. [19] found that when the model resolution increases, the net surface heat fluxes over the area north of 26° N in the Atlantic will be convergent with the observations, and so does the inferred heat transport.

4. Discussion

The developed DEEPC data set [1,5,7,11] has been widely used in the climate research community [8,13,38–48]. The reconstructed TOA radiative fluxes are regarded as "high confidence" by the IPCC AR6 report [16]. However, the large uncertainty of 0.61 Wm^{-2} over the reconstructed period from 1985–1999 should be further improved. This large uncertainty is mainly from the spread of the AMIP6 simulations at the discontinuity points around 1999, and will significantly affect the uncertainty range of the ocean heat content derived from the net TOA flux F_T. This can be further improved by using ensemble runs from a high-quality AMIP model, such as the UK Met Office HadGEM model. This work is ongoing.

The verification of the DEEPC data has been mainly over ocean areas [19,47]. The comparison with observations showed that the bias of the oceanic energy budget in the north Atlantic is within -0.2 (2.7) Wm^{-2} for the period 2005–2009 using estimated DEEPC surface fluxes with (without) land flux adjustment, and the inferred fluxes on station-scale can reach a mean bias of -20.1 Wm^{-2} when buoy-based fluxes are compared. However, the F_s over land is still not well validated. Figure 5 shows the snowmelt effect on the relationship between the net surface energy flux and the surface temperature change ΔT at a location (22° W, 64° N) in Iceland. ΔT is the temperature difference between two adjacent months (e.g., the April F_s versus the temperature change between April and March). It can be seen that before the energy needed for snowmelt (F_{snow}) is considered, the correlation coefficient is only 0.25 for data in all months, and it is improved significantly to 0.83 after F_{snow} is considered. Similarly, the vegetation type and soil moisture, as well as other surface condition changes, also influence this relationship. Therefore, a more complicated land surface energy budget model should be built for this study in order to improve the accuracy of the land surface energy flux F_s. As found by Mayer et al. [47], the surface flux F_s bias on the regional scale is large. The latest study by Kato et al. [49] also showed that the hydrometeor transport and water mass imbalance could affect the enthalpy flux, and the water phase change can influence the diabatic heating rate over the regional ocean areas. Their results indicated that the change in the regional diabatic heating rate could reach 15 Wm^{-2} due to the precipitation phase change. Therefore, on the regional scale, these water phase changes may need careful treatment. On the global scale, Trenberth and Fasullo [50] developed a new method to deal with the hydrological cycle. The water mass (precipitation and evaporation) is redistributed to guarantee the correct atmospheric divergence calculation. However, their inferred meridional heat transport at 26° N north Atlantic is still lower than the RAPID observations, indicating the underestimation of the derived surface fluxes over the Atlantic, mainly due to the unrealistic land surface fluxes. Therefore, land flux adjustment is still necessary.

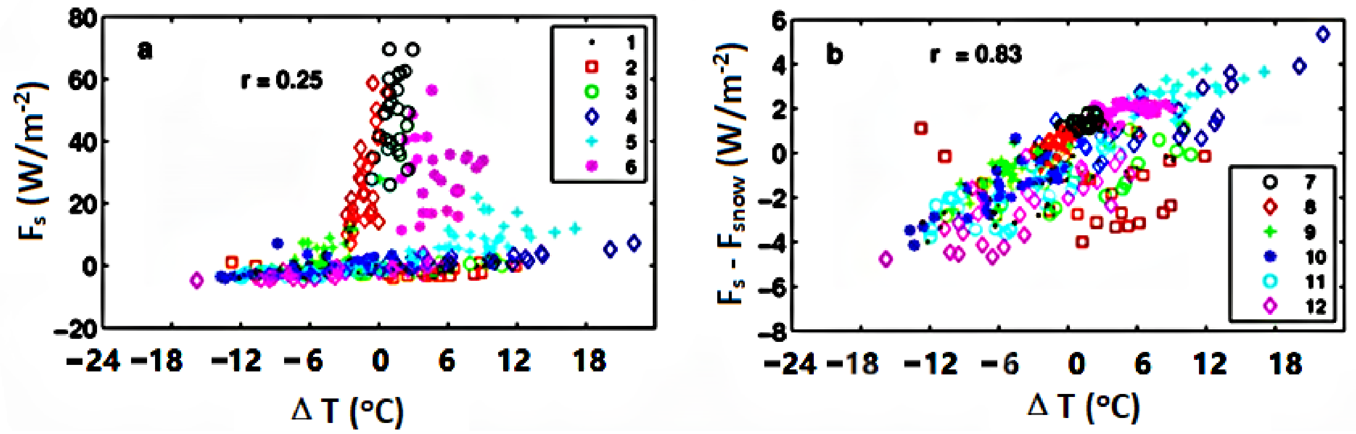

Figure 5. (**a**) Scatter plot between the net surface energy flux F_s and surface temperature change ΔT at a land location for each month (1–12 means JAN-DEC). (**b**) Scatter plot between $F_s - F_{snow}$ and surface temperature change ΔT. F_s (W/m^{-2}) $F_s - F_{snow}$ (W/m^{-2}) ΔT (°C).

5. Conclusions

Climate change is essentially caused by the imbalance of the energy budget in the Earth system. This energy budget imbalance can affect both the global and regional scales through energy transportation by atmospheric circulation. There are still large uncertainties in the estimation of the energy fluxes and transport from both observations and model simulations; progress has been made in recent years. This paper briefly reviews the reconstructed energy fluxes at TOA and the estimated net surface fluxes. The procedures for the data retrieval are described, and the results are compared with other data sets.

Under the constraint of observations, the radiative fluxes at TOA have been reconstructed prior to CERES between 1985 and 2000; together with the CERES satellite observations, the radiative fluxes at TOA from 1985 onwards are provided and can be used in the climate change research. After the mass imbalance in ERA5 atmospheric reanalysis is corrected using a newly developed method considering the enthalpy removal of the atmospheric water vapor [12,13], the total atmospheric energy divergence can be accurately calculated. Meanwhile, the freshwater flux balances at the surface are ensured. The net surface energy flux (F_s) has been estimated using the residual method (the net TOA radiative fluxes minus the atmospheric energy tendency and divergence) based on energy conservation, which is the most reliable method so far [8,14]. The F_s is then verified directly and indirectly with observations, and results show that the estimated F_s in North Atlantic is superior to those from model simulations.

This paper gives a brief review of the progress in the estimation of the observed energy flow in the Earth system, discusses some caveats of the existing method, and provides some suggestions for the improvements of the aforementioned data sets. On the one hand, mass imbalance in the current atmospheric reanalysis is still a problem, and it is expected to apply the mass correction to the data assimilation step to improve the mass divergence calculation, therefore obtaining more accurate energy transport data. On the other hand, with the rapid development of the model simulation and data assimilation technique, as well as the modification of model formulations, the atmospheric mass and energy transport datasets are expected to be more accurate than existing ones in the next generation of atmospheric reanalysis. As discussed above, extensive comparisons and verifications using DEEPC data have been conducted over oceans. However, there is still little verification over land regions. The future work will be focused on solving the existing problems discussed in Section 4 and making more verifications over land regions in order to provide accurate, useful datasets for the research community.

Author Contributions: Conceptualization, C.L., J.L. and N.C. (Ning Cao); methodology, C.L. and N.O.; software, N.C. (Ni Chen) and N.O.; formal analysis, N.C. (Ni Chen), C.L. and Y.Y.; writing—original draft preparation, C.L., N.C. (Ni Chen), J.L. and N.C. (Ning Cao); writing—review and editing C.L., N.C. (Ni Chen), J.L., N.C. (Ning Cao), Y.Y. and X.L.; visualization, C.L., N.C. (Ni Chen), L.J., R.Z., K.Y. and Q.S. All authors have read and agreed to the published version of the manuscript.

Funding: This research was jointly funded by the National Natural Science Foundation of China (442275017, 2075036); Fujian Key Laboratory of Severe Weather (2021KFKT02); the scientific research start-up grant of Guangdong Ocean University (R20001); the Postgraduate Education Innovation Project of Guangdong Ocean University (202144, 202253). Chunlei Liu is also supported by the University of Reading as a visiting fellow. Xiaoqing Liao and Yazhu Yang are also supported by the Postgraduate Education Innovation Project of Guangdong Ocean University (202144, 202253).

Data Availability Statement: The DEEPC data can be downloaded from https://researchdata.reading.ac.uk/347/ (accessed on 26 October 2021), The ORAS5 data from https://www.cen.uni-hamburg.de/icdc/data/ocean/easy-init-ocean/ecmwforas5.html (accessed on 2 January 2020), the RAPID data from https://rapid.ac.uk/rapidmoc/rapid_data/datadl.php (accessed on 22 December 2020), and the AMIP6 data from https://esgfnode.llnl.gov/projects/cmip6/ (accessed on 6 October 2021). We acknowledge all teams and climate modeling groups for making their data available.

Acknowledgments: We thank Michael Mayer and Johannes Mayer for providing the latest mass-corrected ERA5 atmospheric energy divergences. We also thank the ECMWF for providing the ERA5 atmospheric reanalysis data.

Conflicts of Interest: The authors declare no conflict of interest.

References

1. Allan, R.P.; Liu, C.; Loeb, N.B.; Palmer, M.D.; Roberts, M.; Smith, D.; Vidale, P.-L. Changes in global net radiative imbalance 1985–2012. *Geophys. Res. Lett.* **2014**, *41*, 5588–5597. [CrossRef] [PubMed]
2. Loeb, N.G.; Lyman, J.M.; Johnson, G.C.; Allan, R.; Doelling, D.R.; Wong, T.; Soden, B.; Stephens, G.L. Observed changes in top-of-atmosphere radiation and upper-ocean heating consistent within uncertainty. *Nat. Geosci.* **2012**, *5*, 110–113. [CrossRef]
3. Wong, T.; Wielicki, B.A.; Lee, R.B.; Smith, G.L.; Bush, K.A.; Willis, J.K. Reexamination of the observed decadal variability of the earth radiation budget using altitude-corrected ERBE/ ERBS nonscanner WFOV data. *J. Clim.* **2006**, *19*, 4028–4040. [CrossRef]
4. Dee, D.P.; Uppala, S.M.; Simmons, A.J.; Berrisford, P.; Poli, P.; Kobayashi, S.; Andrae, U.; Balmaseda, M.A.; Balsamo, G.; Bauer, P.; et al. The ERA-Interim reanalysis: Confguration and performance of the data assimilation system. *Q. J. R. Meteorol. Soc.* **2011**, *137*, 553–597. [CrossRef]
5. Liu, C.; Allan, R.P.; Mayer, M.; Hyder, P.; Loeb, N.; Roberts, C.D.; Edwards, J.M.; Vidale, P.-L. Evaluation of satellite and reanalysisbased global net surface energy flux and uncertainty estimates. *J. Geophys. Res. Atmos.* **2017**, *122*, 6250–6272. [CrossRef]
6. Hersbach, H.; Bell, B.; Berrisford, P.; Hirahara, S.; Horanyi, A.; Muñoz-Sabater, J.; Nicolas, J.; Peubey, C.; Radu, R.; Schepers, D.; et al. The ERA5 global reanalysis. *Q. J. R. Meteorol. Soc.* **2020**, *146*, 1999–2049. [CrossRef]

7. Liu, C.; Allan, R.P.; Mayer, M.; Hyder, P.; Desbruyères, D.; Cheng, L.; Xu, J.; Xu, F.; Zhang, Y. Variability in the global energy budget and transports 1985−2017. *Climate Dyn.* **2020**, *55*, 3381–3396. [CrossRef]
8. Trenberth, K.E.; Zhang, Y.; Fasullo, J.T.; Cheng, L. Observationbased estimates of global and basin ocean meridional heat transport time series. *J. Clim.* **2019**, *32*, 4567–4583. [CrossRef]
9. Trenberth, K.E. Climate diagnostics from global analyses: Conservation of mass in ECMWF analyses. *J. Clim.* **1991**, *4*, 707–722. [CrossRef]
10. Mayer, M.; Haimberger, L. Poleward atmospheric energy transports and their variability as evaluated from ECMWF reanalysis data. *J. Clim.* **2012**, *25*, 734–752. [CrossRef]
11. Liu, C.; Allan, R.P.; Berrisford, P.; Mayer, M.; Hyder, P.; Loeb, N.; Smith, D.; Vidale, P.-L.; Edwards, J.M. Combining satellite observations and reanalysis energy transports to estimate global net surface energy fluxes 1985–2012. *J. Geophys. Res. Atmos.* **2015**, *120*, 9374–9389. [CrossRef]
12. Mayer, M.; Haimberger, L.; Edwards, J.M.; Hyder, P. Toward consistent diagnostics of the coupled atmosphere and ocean energy budgets. *J. Clim.* **2017**, *30*, 9225–9246. [CrossRef]
13. Mayer, J.; Mayer, M.; Haimberger, L. Consistency and homogeneity of atmospheric energy, moisture, and mass budgets in ERA5. *J. Clim.* **2021**, *34*, 3955–3974. [CrossRef]
14. Trenberth, K.E.; Zhang, Y. Observed interhemispheric meridional heat transports and the role of the Indonesian throughfow in the Pacifc Ocean. *J. Clim.* **2019**, *32*, 8523–8536. [CrossRef]
15. Trenberth, K.E.; Solomon, A. The global heat balance: Heat transports in the atmosphere and ocean. *Clim. Dyn.* **1994**, *10*, 107–134. [CrossRef]
16. Arias, P.; Bellouin, N.; Coppola, E.; Jones, R.; Krinner, G.; Marotzke, J.; Zickfeld, K. Technical Summary. In *Climate Change 2021: The Physical Science Basis. Contribution of Working Group I to the Sixth Assessment Report of the Intergovernmental Panel on Climate Change*; Masson-Delmotte, V., Ed.; Cambridge University Press: Cambridge, UK, 2021; *in press*.
17. Smeed, D.; McCarthy, G.; Rayner, D.; Moat, B.I.; Johns, W.E.; Baringer, M.O.; Meinen, C.S. Atlantic Meridional Overturning Circulation Observed by the RAPID-MOCHA-WBTS (RAPID-Meridional Overturning Circulation and Heatfux Array-Western Boundary Time Series) Array at 26N from 2004 to 2017; British Oceanographic Data Centre, Natural Environment Research Council. 2017. Available online: https://rmets.onlinelibrary.wiley.com/doi/abs/10.1002/qj.828 (accessed on 10 November 2019).
18. Zuo, H.; Balmaseda, M.A.; Tietsche, S.; Mogensen, K.; Mayer, M. The ECMWF operational ensemble reanalysis–analysis system for ocean and sea ice: A description of the system and assessment. *Ocean Sci.* **2019**, *15*, 779–808. [CrossRef]
19. Liu, C.; Yang, Y.; Liao, X.; Cao, N.; Liu, J.; Ou, N.; Allan, R.P.; Jin, L.; Chen, N.; Zheng, R. Discrepancies in simulated ocean net surface heat fluxes over the North Atlantic. *Adv. Atmos. Sci.* **2022**, *39*, 1941–1955. [CrossRef]
20. Chiodo, G.; Haimberger, L. Interannual changes in mass consistent energy budgets from ERA-Interim and satellite data. *J. Geophys. Res.* **2010**, *115*, D02112. [CrossRef]
21. Simmons, A.J.; Burridge, D.M. An energy and angular-momentum conserving vertical finite-difference scheme and hybrid vertical coordinates. *Mon. Weather Rev.* **1981**, *109*, 758–766. [CrossRef]
22. Loeb, N.G.; Wang, H.L.; Cheng, A.N.; Kato, S.; Fasullo, J.T.; Xu, K.-M.; Allan, R.P. Observational constraints on atmospheric and oceanic cross-equatorial heat transports: Revisiting the precipitation asymmetry problem in climate models. *Clim. Dyn.* **2016**, *46*, 3239–3257. [CrossRef]
23. Trenberth, K.E.; Fasullo, J.T. Atlantic meridional heat transports computed from balancing Earth's energy locally. *Geophys. Res. Lett.* **2017**, *44*, 1919–1927. [CrossRef]
24. Loeb, N.G.; Doelling, D.R.; Wang, H.; Su, W.; Nguyen, C.; Corbett, J.G.; Liang, L.; Mitrescu, C.; Rose, F.G.; Kato, S. Clouds and the earth's radiant energy system (CERES) energy balanced and flled (EBAF) top-of-atmosphere (TOA) edition 4.0 data product. *J. Clim.* **2018**, *31*, 895–918. [CrossRef]
25. Wu, T.; Yu, R.; Lu, Y.; Jie, W.; Fang, Y.; Zhang, J.; Zhang, L.; Xin, X.; Li, L.; Wang, Z.; et al. BCC-CSM2-HR: A high-resolution version of the Beijing Climate Center Climate System Model. *Geosci. Model Dev.* **2021**, *14*, 2977–3006. [CrossRef]
26. Danabasoglu, G.; Lamarque, J.-F.; Bacmeister, J.; Bailey, D.A.; DuVivier, A.K.; Edwards, J.; Emmons, L.K.; Fasullo, J.; Garcia, R.; Gettelman, A.; et al. The Community Earth System Model Version 2 (CESM2). *J. Adv. Model. Earth Syst.* **2020**, *12*, e2019MS001916. [CrossRef]
27. Eyring, V.; Bony, S.; Meehl, G.A.; Senior, C.A.; Stevens, B.; Stouffer, R.J.; Taylor, K.E. Overview of the Coupled Model Intercomparison Project Phase 6 (CMIP6) experimental design and organization. *Geosci. Model Dev.* **2016**, *9*, 1937–1958. [CrossRef]
28. Davini, P.; von Hardenberg, J.; Corti, S.; Christensen, H.M.; Juricke, S.; Subramanian, A.; Watson, P.A.G.; Weisheimer, A.; Palmer, T.N. Climate SPHINX: Evaluating the impact of resolution and stochastic physics parameterisations in the EC-Earth global climate model. *Geosci. Model Dev.* **2017**, *10*, 1383–1402. [CrossRef]
29. He, B.; Liu, Y.; Wu, G.; Bao, Q.; Zhou, T.; Wu, X.; Wang, L.; Li, J.; Wang, X.; Li, J.; et al. CAS FGOALS-f3-L model datasets for CMIP6 GMMIP Tier-1 and Tier-3 experiments. *Adv. Atmos. Sci.* **2020**, *37*, 18–28. [CrossRef]
30. Williams, K.D.; Harris, C.M.; Bodassalcedo, A.; Camp, J.; Comer, R.E.; Copsey, D.; Fereday, D.; Graham, T.; Hill, R.; Hinton, T.; et al. The Met Ofce Global Coupled model 2.0 (GC2) confguration. *Geosci. Model Dev.* **2015**, *88*, 1509–1524. [CrossRef]
31. Boucher, O.; Denvil, S.; Levavasseur, G.; Cozic, A.; Caubel, A.; Foujols, M.-A.; Meurdesoif, Y.; Ghattas, J. IPSL IPSL-CM6A-LR model output prepared for CMIP6 HighResMIP. *Earth Syst. Grid Fed.* **2019**. [CrossRef]

32. Tatebe, H.; Ogura, T.; Nitta, T.; Komuro, Y.; Ogochi, K.; Takemura, T.; Sudo, K.; Sekiguchi, M.; Abe, M.; Saito, F.; et al. Description and basic evaluation of simulated mean state, internal variability, and climate sensitivity in MIROC6. *Geosci. Model Dev.* **2019**, *12*, 2727–2765. [CrossRef]
33. Yukimoto, S.; Kawai, H.; Koshiro, T.; Oshima, N. The Meteorological Research Institute Earth System Model version 2.0, MRI-ESM2.0: Description and basic evaluation of the physical component. *J. Meteor. Soc. Jpn.* **2019**, *97*, 931–965. [CrossRef]
34. Park, S.; Shin, J.; Kim, S.; Oh, E. Global Climate Simulated by the Seoul National University Atmosphere Model Version 0 with a Unified Convection Scheme (SAM0-UNICON). *J. Clim.* **2019**, *32*, 2917–2949. [CrossRef]
35. Cheng, L.J.; Trenberth, K.E.; Fasullo, J.; Boyer, T.; Abraham, J.; Zhu, J. Improved estimates of ocean heat content from 1960 to 2015. *Sci. Adv.* **2017**, *3*, e1601545. [CrossRef] [PubMed]
36. Gentine, P.; Seneviratne, S.I.; Beltrami, H.; Davin, E.; Meier, R.; García-García, A.; Cuesta-Valero, F.J. Large recent continental heat storage. In *AGU Fall Meeting Abstracts*; American Meteorological Society: San Francisco, CA, USA, 2019; Volume 2019, p. GC51J-1078.
37. Terai, C.R.; Caldwell, P.M.; Klein, S.A.; Tang, Q.; Branstetter, M.L. The atmospheric hydrologic cycle in the ACME v0.3 model. *Clim. Dyn.* **2018**, *50*, 3251–3279. [CrossRef]
38. Qu, J.; Truhan, J.J.; Dai, S.; Luo, H.; Blau, P.J. An assessment of air-sea heat fuxes from ocean and coupled reanalyses. *Clim. Dyn.* **2015**, *22*, 207–214. [CrossRef]
39. Roberts, M.J.; Hewitt, H.T.; Hyder, P.; Ferreira, D.; Josey, S.A.; Mizielinski, M.; Shelly, A. Impact of ocean resolution on coupled airsea fuxes and large-scale climate. *Geophys. Res. Lett.* **2016**, *43*, 10430–10438. [CrossRef]
40. Roberts, C.D.; Palmer, M.D.; Allan, R.P.; Desbruyeres, D.G.; Hyder, P.; Liu, C.; Smith, D. Surface fux and ocean heat transport convergence contributions to seasonal and interannual variations of ocean heat content. *J Geophys. Res Ocean.* **2017**, *122*, 726–744. [CrossRef]
41. Senior, C.A.; Andrews, T.; Burton, C.; Chadwick, R.; Copsey, D.; Graham, T.; Hyder, P.; Jackson, L.; McDonald, R.; Ridley, J.; et al. Idealised climate change simulations with a high resolution physical model: HadGEM3-GC2. *J. Adv. Model Earth Syst.* **2016**, *8*, 813–830. [CrossRef]
42. Hyder, P.; Edwards, J.M.; Allan, R.P.; Hewitt, H.T.; Bracegirdle, T.J.; Gregory, J.M.; Belcher, S.E. Critical Southern Ocean climate model biases traced to atmospheric model cloud errors. *Nat. Commun.* **2018**, *9*, 3625. [CrossRef]
43. Mignac, D.; Ferreira, D.; Haines, K. South Atlantic meridional transports from NEMO-based model simulations and reanalyses. *Ocean Sci.* **2018**, *14*, 53–68. [CrossRef]
44. Cheng, L.; Trenberth, K.E.; Fasullo, J.; Mayer, M.; Balmaseda, M.; Zhu, J. Evolution of ocean heat content related to ENSO. *J. Clim.* **2019**, *32*, 3529–3556. [CrossRef]
45. Allison, L.C.; Palmer, M.D.; Allan, R.P.; Hermanson, L.; Liu, C.L.; Smith, D.M. Observations of planetary heating since the 1980s from multiple independent datasets. *Environ. Res. Commun.* **2020**, *2*, 101001. [CrossRef]
46. Bryden, H.L.; Johns, W.E.; King, B.A.; McCarthy, G.; Mcdonagh, E.L.; Moat, B.I.; Smeed, D.A. Reduction in ocean heat transport at 26° N since 2008 cools the eastern subpolar gyre of the North Atlantic Ocean. *J. Clim.* **2020**, *33*, 1677–1689. [CrossRef]
47. Mayer, J.; Mayer, M.; Haimberger, L.; Liu, C. Comparison of surface energy fluxes from global to local scale. *J. Clim.* **2022**, *35*, 4551–4569. [CrossRef]
48. Andrews, T.; Bodas-Salcedo, A.; Gregory, J.M.; Dong, Y.; Armour, K.C.; Paynter, D.; Lin, P.; Modak, A.; Mauritsen, T.; Cole, J.N.S.; et al. On the effect of historical SST patterns on radiative feedback. *J. Geophys. Res.* **2022**, *87*, 161–177. [CrossRef]
49. Kato, S.; Loeb, N.G.; Fasullo, J.T.; Trenberth, K.E.; Lauritzen, P.H.; Rose, F.G.; Rutan, D.A.; Satoh, M. Regional Energy and Water Budget of a Precipitating Atmosphere over Ocean. *J. Clim.* **2021**, *34*, 4189–4205. [CrossRef]
50. Trenberth, K.E.; Fasullo, J.T. Applications of an updated atmospheric energetics formulation. *J. Clim.* **2018**, *31*, 6263–6279. [CrossRef]